15TH IEA HEAT PUMP CONFERENCE
MAY 26–29, 2026 | HOFBURG VIENNA 2026
DECARBONISATION THROUGH INNOVATION

Thermophysical Property Characterization of R1336mzz(Z) with POE 380 for High-Temperature Heat Pump Applications

Ganesh B. Venkatesan*, Madison P. Ward, Riley B. Barta

Ray W. Herrick Laboratories, School of Mechanical Engineering, Purdue University, West Lafayette, IN, 47901, USA

Abstract

As the global demand for decarbonized heating solutions intensifies, high-temperature heat pumps (HTHPs) have emerged as a promising alternative to fossil fuel-based industrial heating. In response to evolving environmental regulations, the need for low global warming potential (GWP) refrigerants that can sustain efficient operation at elevated temperatures has grown significantly. While some low-GWP refrigerants demonstrate favourable thermodynamic properties for high-temperature applications, their lubricant compatibility and thermophysical behaviour under extreme conditions remain underexplored. This study aims to address this gap in the literature by utilizing a high temperature thermophysical property measurement setup, capable of operation up to 190 °C. Using this test setup, the thermophysical properties of R1336mzz(Z), a promising high temperature, low-GWP refrigerant, was experimentally characterized in combination with polyol ester (POE) 380 lubricant. Key parameters such as saturation pressure, density, and viscosity were measured over refrigerant mass fractions ranging from 0.55 to 0.9 across a range of temperatures up to 160 °C. To enhance the usability of the experimental dataset, established empirical viscosity, density, and pressure correlations including the ASTM blending rule were applied, and new coefficient sets were determined for the R1336mzz(Z)–POE 380 mixture. These calibrated correlations provide reliable property predictions as functions of temperature and refrigerant mass fractions. The resulting models enable accurate component-level analyses and full-cycle simulations of high-temperature heat pump systems operating with low-GWP refrigerant–lubricant mixtures, thereby supporting ongoing efforts toward decarbonized industrial heating.

Selection and/or peer-review under the responsibility of the organizers of the 15th IEA Heat Pump Conference 2026.

Keywords: Refrigerant–lubricant interaction; Thermophysical properties; Low-GWP refrigerant; High-temperature heat pump (HTHP)

1. Introduction

Industrial heat accounts for roughly one-quarter of global final energy use and CO_2 emissions [1]. A large share of this demand is concentrated in medium and high-temperature processes such as drying, pasteurization, sterilization, pulp and paper production, food processing, chemical synthesis, and steam generation, currently supplied by fossil-fuel boilers or direct combustion of natural gas and coal [2,3,4]. These systems emit substantial greenhouse gases and air pollutants, making them a critical focus area for climate policy under the Paris Agreement [2] and the EU Green Deal [1].

High-temperature heat pumps (HTHPs) offer a compelling alternative to fossil-based industrial heating by recovering low-grade waste heat and upgrading it to temperatures suitable for process use (typically 80–165 °C) [5]. By electrifying heat and reducing fossil fuel consumption, HTHPs can cut equivalent CO_2 emissions by up to 68 % compared to natural gas boilers [3]. The choice of refrigerant strongly influences the feasible

* Corresponding author. Tel.: +1-765-543-8688
E-mail address: gbramman@purdue.edu

temperature lift, efficiency, and environmental footprint of an HTHP. Historically, high-Global Warming Potential (GWP) fluids, such as R245fa, dominated industrial systems [2]. In response to F-gas regulations and the Kigali Amendment, fourth-generation refrigerants, including hydrofluoroolefins (HFOs) like R1336mzz(Z) and hydrocarbons like cyclopentane, have emerged as promising low-GWP alternatives [6]. These fluids offer high critical temperatures, making them attractive for high-temperature applications. Yet, despite growing adoption in prototype systems, the thermophysical behavior of these refrigerants in combination with lubricants under extreme conditions remains underexplored [7]. This is primarily due to the limited availability of experimental infrastructure capable of handling high-temperature refrigerant–lubricant mixtures in the temperature range of 140–200 °C.

Lubricants are indispensable in compressors for friction reduction, sealing, and heat removal. However, lubricant circulation affects every component of a vapor compression system, from compressor performance to heat exchanger efficiency [8]. In the compressor sump, the refrigerant can dissolve partially or extensively in the lubricant depending on the system pressure, temperature, and the chemical nature of both fluids. This dissolution alters the lubricant viscosity, density, and solubility characteristics, directly influencing bearing lubrication, film stability, and sealing integrity. A portion of the lubricant inevitably escapes the compressor discharge and circulates through the system. When phase separation occurs in the heat exchangers, especially in evaporators, where temperatures and pressures are lowest, lubricant can accumulate on heat-transfer surfaces, reducing efficiency and hindering return flow. At the same time, excessive refrigerant dilution in the compressor sump lowers lubricant viscosity, increasing wear and the risk of mechanical failure. Developing semi-empirical, non-predictive models of refrigerant–lubricant interactions remain challenging due to the limited compositional knowledge and thermophysical data of commercial lubricants. Synthetic lubricants such as polyol ester (POE) and polyalkylene glycols (PAG) are proprietary blends, typically characterized only by bulk properties such as viscosity and density [9]. The emergence of low-GWP refrigerants, including HFOs and HCFOs, further complicates compatibility assessment. Accurate measurements of viscosity, density, and miscibility across refrigerant mass fractions are therefore essential to develop reliable mixture correlations and ensure stable lubrication, efficient heat transfer, and long-term performance in high-temperature heat pump systems [7, 10].

Testing mixtures at different refrigerant mass fractions is therefore vital, as the solubility of the refrigerant in lubricant varies significantly with composition and temperature, leading to nonlinear effects on viscosity, density, and vapor pressure. Understanding these variations is essential for accurately representing compressor-sump and evaporator conditions in system models. To address this need, the present study utilizes a high-temperature thermophysical property measurement setup capable of operation up to 190 °C. Using this setup, the thermophysical properties of the low-GWP refrigerant R1336mzz(Z) were experimentally investigated in combination with POE 380 lubricant over a range of refrigerant mass fractions representative of compressor and system conditions. Measurements of saturation pressure, density, and dynamic viscosity were performed up to 160 °C to capture the behavior under high-temperature, lubricant-rich environments. To enhance the applicability of these results, empirical coefficients were derived using established correlations widely used in literatures and ASTM blending [12] equations, enabling accurate representation of mixture properties over wide temperature and refrigerant mass fraction ranges. The resulting dataset and correlations provide a foundational framework for next-generation component models and full-cycle HTHP simulations operating with low-GWP refrigerant–lubricant mixtures.

2. Methodology

2.1. Refrigerant and lubricant selection

An extensive refrigerant screening study [5] was conducted for HTHP applications, incorporating rigorous selection criteria to ensure thermodynamic suitability, safety, and environmental compliance. The screening excluded fluids with a critical temperature less than 125 °C or a saturation pressure at 40 °C lower than 0.05 bar(a). In addition, compounds with ozone-depleting potential (ODP > 0) or a 100-year global warming potential (GWP_{100} > 1000) were filtered out. Further considerations included flammability and toxicity in accordance with ASHRAE Standard 34 [14], chemical stability as defined by the National Fire Protection Association (NFPA), as well as autoignition temperatures below 250 °C. Cycle analyses were performed across a range of source and sink temperature conditions to evaluate performance. Based on these evaluations,

synthetic refrigerants such as R1336mzz(Z), R1234ze(Z), R1233zd(E) and R1224yd(Z) were identified as promising candidates for higher volumetric heat capacity due to their low toxicity and minimal flammability.

A comparative summary of the thermophysical, environmental, and safety characteristics of the evaluated high-temperature refrigerants relative to R245fa is presented in Table 1. Among the synthetic low-GWP candidates, R1336mzz(Z) demonstrates higher suitability for extreme high-temperature applications, primarily due to its higher critical temperature compared to other alternatives. Accordingly, a comprehensive understanding of the thermophysical behavior of R1336mzz(Z) with compatible lubricants is critically important to enable reliable design and optimization of next-generation HTHP systems.

Table 1. Comparison of thermophysical, environmental and safety properties of different high temperature refrigerants

Property	R245fa	R1234ze(Z)	R1233zd(E)	R1224yd(Z)	R1336mzz(Z)
Molecular structure	$C_3H_3F_5$	$C_3H_2F_4$	$C_3ClH_2F_3$	C_3ClHF_4	$C_4H_2F_6$
Molecular mass [kg/kmol]	134	114.0416	130.5	148.5	164.1
Critical temperature [C]	153.9	150.12	166.5	155.5	171.3
Critical Pressure [bar]	36.5	35.33	36.2	33.4	29.0
Normal boiling point [C]	15	9.75	18	15	33
ODP	0	0	0.00024	0.00023	0
GWP_{100}	1030	<1	1	0.88	2
Atmospheric life time	7.7 y	10 d	26 d	20 d	22 d
ASHRAE safety classification	B1	A2L	A1	A1	A1

HFO refrigerants are compatible with synthetic lubricants compared to mineral lubricants. PAG and POE lubricants are predominantly employed in the refrigeration and air conditioning industry for HFO refrigerants. This study specifically investigates the thermophysical properties of R1336mzz(Z) with POE 380 lubricant. The use of high viscosity grade lubricant is intended to understand the behavior at high temperature conditions.

2.2. Experimental setup

The experimental setup shown in Figure 1 utilizes a recirculation loop method to investigate the thermophysical properties of refrigerant and lubricant mixtures under controlled conditions, as detailed in [16]. A variable-speed pump circulated the fluid, ensuring precise control of flow rate and uniformity throughout the system. Temperature measurements were obtained using a PT100 RTD with Class A accuracy, known for its high precision and stability. Pressure measurements were recorded using Rosemount pressure transmitters equipped with diaphragm seals and capillary tubes. To achieve higher accuracy, two different pressure transmitters were employed, covering ranges of 0 to 55 bar(a) and 0 to 275 bar(a), as the measurement accuracy dependent on the span of the transmitter. Viscosity was measured using an oscillating piston viscometer, which provided the advantage of sampling fresh fluid with each oscillation, thereby enhancing measurement accuracy. The viscometer was equipped with two interchangeable pistons, enabling measurement across a broad viscosity range from 0.25 to 50 cP. Coriolis type mass flow meter was employed in the loop to record fluid density. Additionally, a bypass valve was used to facilitate fluid agitation, ensuring homogeneous mixing of the refrigerant and lubricant while maintaining a minimum flow rate to safeguard the pump from cavitation and accelerate the rate at which thermodynamic equilibrium of the mixtures being assessed is achieved. The mass of the charged lubricant and refrigerant was measured using a high-precision laboratory scale with an accuracy of ± 0.01 g. To maintain safe operational conditions, an adjustable pressure relief valve was integrated into the system to prevent over-pressurization. Given the potential flammability of certain refrigerant mixtures, a nitrogen purge system was installed to create an inert atmosphere within the test chamber, significantly reducing the risk of combustion by lowering the oxygen concentration within the chamber. The setup adheres to ASHRAE 15 and 34 standards [13,14] ensuring safe refrigerant handling. In the event of flammable refrigerant leaks, the refrigerant will safely vent out through the exhaust vent from the chamber into a well-ventilated area. Even the maximum charge levels of up to 1.2 kg remained well below the maximum charge limits calculated using ASHRAE standards for the area in which the chamber is located. The measurement

uncertainties of applied measurement devices are summarized in Table 2. The internal volume of the test setup was determined by isothermal gas method and found to be 1449 cm^3.

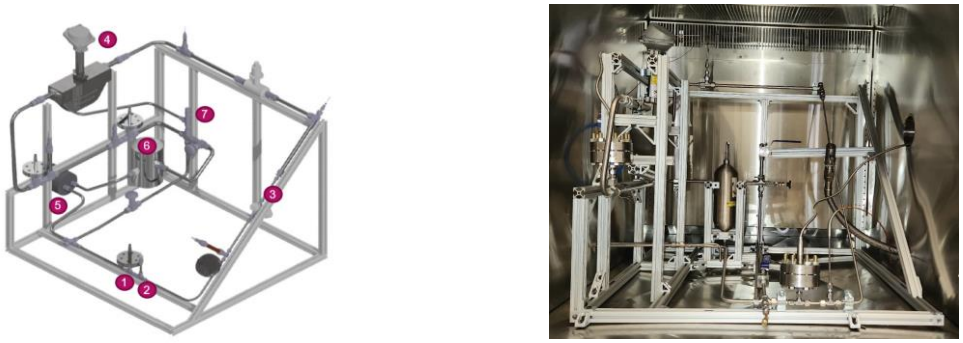

(a) (b)

Figure 1. Rendered model (a) and photo (b) of the experimental setup: 1. Pressure transmitter, 2. Temperature, 3. Viscometer, 4. Mass flow meter, 5. Gear pump, 6. Liquid receiver, 7. Pressure relief valve

Table 2. Uncertainty of measurement values

Measurement	Range	Measurement Uncertainty
Pressure	0 to 55 bar(a), 0 to 275 bar(a)	± 0.075 % of span
Temperature	-100 to 450 ºC	± (0.15 + 0.002·T) ºC
Mass flow	0 to 1336 kg/hr	± 0.2 % reading
Liquid Density	-	± 2 kg/m³
Liquid Viscosity	0.25 to 5 cP, 5 to 50 cP	1 % of span

2.3. Operation

A Piping and Instrumentation Diagram (P&ID) of the test setup is provided in Figure 2. The experimental setup is prepared by first flushing with a volatile solvent, followed by nitrogen purging, and then evacuating the test stand to a vacuum level. Initially, the lubricant is charged into the system using charging port (12). The mass before and after charging lubricant is noted and the system is evacuated again. The refrigerant is then charged into a sample cylinder along with the charging hose, which is weighed (m_1) before charging to the experimental setup. The refrigerant is then transferred to the experimental setup through the charging port (9). To facilitate faster charging, the chamber is cooled by approximately 10 to 15 °C to create a larger pressure differential between the measured refrigerant transfer container and the test setup. Once the charging process is completed, the charging port (9) and the ball valve at the end of the charging hose are closed to isolate the system. The sample cylinder and the charging hose which retain some refrigerant and are therefore weighed again (m_2) after this process. The amount of refrigerant charged into the system is calculated by the difference in weight before and after charging. The gear pump is then switched on and the property measurements are carried out. The test setup was validated through experiments with both pure refrigerants and refrigerant-lubricant mixtures, with results benchmarked against REFPROP [15] data and existing literature.

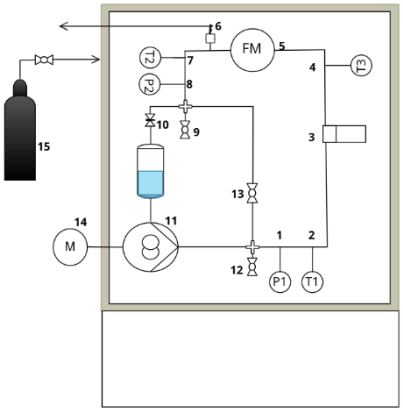

Figure 2. P&ID of the experimental setup: 1. Pressure transmitter 1, 2. RTD 1 at flow inlet, 3. Viscometer, 4. Thermocouple, 5. Mass flow meter, 6. Pressure relief valve, 7. RTD 2, 8. Pressure transmitter 2, 9. Charging valve, 10. Needle valve, 11. Gear pump, 12. Charging valve, 13. Bypass valve, 14. Motor, 15. Nitrogen cylinder for purging

2.4. Vapor space correction

Vapor space correction needs to be performed to account for the portion of refrigerant existing in the vapor phase within the test setup, ensuring that the liquid-phase composition is accurately determined. The vapor-phase mass (1) is estimated using the total system volume, measured liquid density, and vapor density and pressure obtained from REFPROP. The corrected liquid refrigerant mass fraction (2) is then calculated by subtracting the vapor-phase refrigerant mass from the total refrigerant charge. This correction becomes increasingly important at higher temperatures, where vapor formation is more significant, and ensures that the reported liquid-phase composition truly represents the refrigerant–lubricant mixture under test conditions.

$$m_{vapor} = \left(V_{system} - \frac{m_{total}}{\rho_{liquid}}\right) \Big/ \left(\frac{1}{\rho_{vapor}} - \frac{1}{\rho_{liquid}}\right) \quad (1)$$

$$\omega_{refrigerant} = \frac{m_{refrigerant} - m_{vapor}}{m_{lubricant} + m_{refrigerant} - m_{vapor}} \quad (2)$$

In these expressions, $\omega_{refrigerant}$ represents the corrected liquid-phase refrigerant mass fraction, $m_{refrigerant}$ denotes the total refrigerant mass charged into the system, $m_{lubricant}$ refers to the total mass of lubricant added to the test setup. The parameter m_{vapor} corresponds to the mass of refrigerant existing in the vapor phase, V_{system} represents the total internal volume of the test setup, ρ_{liquid} denotes the measured liquid density and ρ_{vapor} denotes the refrigerant vapor density calculated using REFPROP.

3. Modelling

The experimentally measured data are presented in tabular form, graphical form and through empirical correlations. To describe the dependence of the measured properties on operating conditions, empirical correlations are used as a function of two independent variables: temperature and refrigerant mass fraction. The relationships among viscosity, pressure, and density with respect to temperature and refrigerant mass fraction were formulated using the linear regression empirical correlations widely used in literatures. Furthermore, the viscosity–temperature behavior of the mixtures was also modeled using the ASTM blending rule, and the predictions from this model were compared with those obtained from the linear regression correlations. A detailed comparison and discussion of the two modeling approaches are provided to evaluate their accuracy and applicability across the investigated temperature and composition ranges.

3.1. Saturation pressure correlation

An empirical log–log regression model (3) previously adopted in the literature [17], was used to correlate the saturation pressure as a function of temperature and refrigerant mass fraction over the complete experimental range. This single correlation effectively captures the entire data range, encompassing a wide temperature span of approximately 120 °C and varying mixture compositions.

$$log_{10}(P) = \left(a_1 + \frac{a_2}{T} + \frac{a_3}{T^2}\right) + log_{10}(\omega)\left(a_4 + \frac{a_5}{T} + \frac{a_6}{T^2}\right) + log_{10}^{n}(\omega)\left(a_7 + \frac{a_8}{T} + \frac{a_9}{T^2}\right) \quad (3)$$

where, P is the saturation pressure in bar, ω is the refrigerant mass fraction, T is the temperature in K, n is the concentration coefficient and $a_1 - a_9$ are empirical coefficients.

3.2. Density correlation

The measured density was characterized using the Henderson [11] formulation that expresses density variation as a function of temperature and refrigerant mass fraction. Separate empirical correlations were developed for the low and high refrigerant mass fraction regions to accurately capture the differing thermodynamic and transport behaviors of the mixture. This two-region treatment provides improved model fidelity, as the physical mechanism governing solubility and dilution differ significantly between these regions.

For low refrigerant concentration mixtures ($0.55 < \omega < 0.7$):

$$\rho = (a_1 + a_2 T + a_3 T^2) + \omega (a_4 + a_5 T + a_6 T^2) + \omega^2 (a_7 + a_8 T + a_9 T^2) \quad (4)$$

For high refrigerant concentration mixtures ($\omega \geq 0.7$):

$$\rho = (a_1 + a_2 T_r + a_3 T_r^2) + \omega(a_4 + a_5 T_r + a_6 T_r^2) + \omega^2(a_7 + a_8 T_r + a_9 T_r^2) \quad (5)$$

where, ρ is the mixture liquid density in g/cm^3, ω is the refrigerant mass fraction, T is the temperature in K, T_c is the critical temperature in K, $T_r = (1 - T/T_c)$, n is the concentration coefficient and $a_1 - a_9$ are empirical coefficients.

3.3. Viscosity correlation

3.3.1. Empirical log-log correlation model

The measured viscosity was characterized using the empirical log-log relation, similar to the pressure, and due to huge variation of the viscosity with varying temperature ranges and the refrigerant mass fraction ranges, the entire regime is divided to low mass fraction regime ($0.55 < \omega < 0.7$) and high refrigerant mass fraction regime ($\omega \geq 0.7$) to capture the thermodynamic behavior with higher accuracy. As a result, two sets of coefficients are developed for the corresponding regimes.

$$log_{10}(\nu_{mix}) = \left(a_1 + \frac{a_2}{T} + \frac{a_3}{T^2}\right) + log_{10}(\omega)\left(a_4 + \frac{a_5}{T} + \frac{a_6}{T^2}\right) + log_{10}^{n}(\omega)\left(a_7 + \frac{a_8}{T} + \frac{a_9}{T^2}\right) \quad (6)$$

where, ν_{mix} is the mixture kinematic viscosity in cSt, ω is the refrigerant mass fraction, T is the temperature in K, n is the concentration coefficient and $a_1 - a_9$ are empirical coefficients

3.3.2. ASTM blending model

The viscosity–temperature relationship of the refrigerant–lubricant mixtures was also characterized using the ASTM viscosity blending rule, which provides an empirical framework to predict mixture viscosity based on the viscosities of the individual components and their respective mass fractions. The mixture kinematic viscosity is expressed as a logarithmic–Bessel function relationship involving the pure component constants A_i and B_i determined from temperature-dependent viscosity data. The constants for the pure refrigerant were obtained from REFPROP-generated viscosity data across the investigated temperature range, while the corresponding constants for the pure lubricant were back-calculated iteratively using the measured mixture

data. The ASTM model offers a semi-predictive means to estimate mixture viscosities and serves as a useful comparative framework against the fully empirical correlation.

$$log_e\left(log_e\left(\nu_{mix} + 0.7 + e^{-\nu_{mix}} K_0(\nu_{mix} + 1.244067)\right)\right) = \sum_i \omega_i (A_i - B_i \, log_e(T)) \quad (7)$$

where, ν_{mix} is the mixture kinematic viscosity in cSt, ω_i is the mass fraction of the component i, A_i and B_i are the constants for the pure fluid in the mixture, K_0 is the zero-order Bessel function of the second kind, T is the temperature in K.

4. Results and Discussion

The thermophysical properties of R1336mzz(Z)–POE 380 mixtures were measured from 40 °C to 160 °C over a wide range of refrigerant mass fractions largely greater than 0.55. Correlation development and analysis focus on mass fractions greater than 0.55, while a small number of data points at lower mass fractions arise from vapor space effects at high temperatures. The experimental data are presented in tabular form, and empirical correlations were developed based on empirical equations discussed in the previous section to represent the saturation pressure (P), density (ρ), and viscosity (ν) as functions of temperature (T). These models show excellent agreement with the experimental measurements. Furthermore, the viscosity correlations are benchmarked against the ASTM D2501 blending rule, and the two models were compared to evaluate predictive accuracy.

4.1. Empirical coefficients

Table 4 lists the empirical coefficients obtained from fitting the experimental data of R1336mzz(Z)–POE 380 mixtures using the empirical equation (Eq. 3–6). Separate sets of coefficients were determined for low and high refrigerant mass fractions to capture composition-dependent variations in density, and viscosity. In addition, Table 5 presents the empirical coefficients derived for the ASTM D7152 viscosity blending rule from experimental data. These coefficients were used to construct the final correlation models, enabling accurate prediction of thermophysical properties across the measured temperature and composition ranges.

Table 4. Empirical coefficients based on the experimental data (3-6)

		Low refrigerant mass fractions		High refrigerant mass fractions	
Coefficients	Vapor pressure	Density	Viscosity	Density	Viscosity
a1	4.611733719	2.295989579	3.466761e+00	0.228709992	-8.57870135e-01
a2	-1336.386504	-0.008762538	-3.517801e+03	6.422870862	-5.64774522e+01
a3	-28362.16963	1.27E-05	7.103881e+05	-15.98205892	1.79992540e+0
a4	1.862312745	-3.073579579	-3.558278e+00	1.856166195	-1.09113068e+06,
a5	-730.476637	0.025040974	2.420155e+03	-15.86740315	-1.57532682e+06
a6	-14969.56929	-4.05E-05	-7.445398e+05	40.66326791	-1.77327632e+06
a7	7.007458528	2.904013197	-3.752500e+01	-1.23963305	1.09110813e+06
a8	-3966.670188	-0.019319703	2.635729e+04	11.51879387	1.59409292e+06
a9	378952.1927	2.84E-05	-4.579367e+06	-26.21269904	-2.46572470e+06
n	2	-	2	-	1

Table 5. Coefficients for ASTM blending rule equation (7)

Coefficients	R1336mzz(Z)	POE 380
A_1	19.5987	49.39
B_1	3.8060	8.12

4.2. Saturation pressure vs temperature

Figure 3 illustrates the vapor pressure behavior of R1336mzz(Z)–POE 380 mixtures at different refrigerant mass fractions and the accuracy of the empirical model in capturing this trend. In Figure 3(a), the saturation pressure increases exponentially with temperature, and the model predictions for various refrigerant mass fractions closely follow the pure refrigerant curve from REFPROP. As the lubricant content increases (decreasing ω), a greater portion of the refrigerant dissolves in the liquid phase, reducing its availability in the vapor phase. This reduces the mole fraction of the refrigerant in the vapor phase, leading to a lower total system pressure compared to the pure refrigerant. Figure 3(b) presents the deviation between the empirical model predictions and experimental measurements, showing minimal scatter across the entire temperature range. The low mean absolute error (MAE = 0.043 bar), root mean square error (RMSE = 0.067 bar), and a coefficient of determination (R^2 = 0.99) confirm that the empirical model provides a meaningful representation of the experimental saturation pressure data.

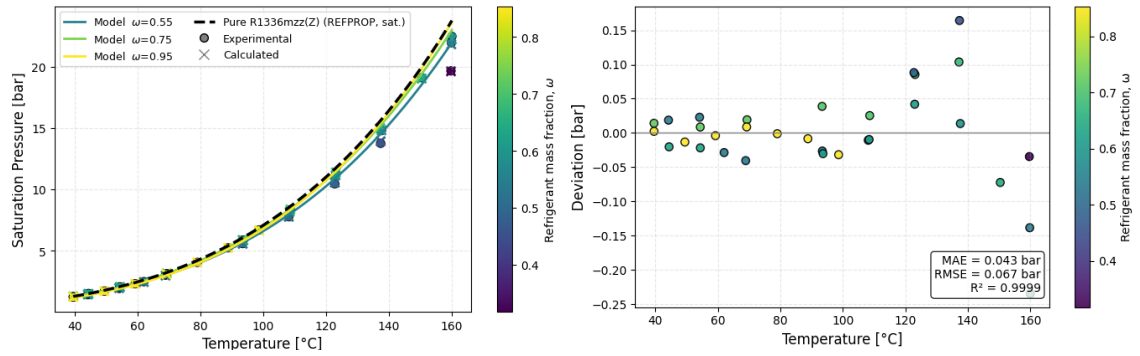

Figure 3. (a) Comparison of experimental and correlated saturation pressures using empirical model (b) Relative deviation between the empirical model predictions and experimental measurements.

4.3. Density vs temperature

Figure 4 shows the variation of liquid density with temperature for pure R1336mzz(Z) with POE 380 mixtures. As expected, the liquid density decreases with the increase in temperatures due to thermal expansion. It can be noted at temperatures below the 120 °C to 140 °C range, the mixtures density is always lower than the pure refrigerant density primarily due the presence of POE 380, which has significantly lower density compared to the pure refrigerant. At the higher end of the temperature range, the density curves approach each other more closely and cross over happens between the pure refrigerant density and mixture densities. This happens due to the difference in expansion rates for the refrigerant and lubricant, and the density of the pure refrigerant drops more rapidly as it nears its critical temperature.

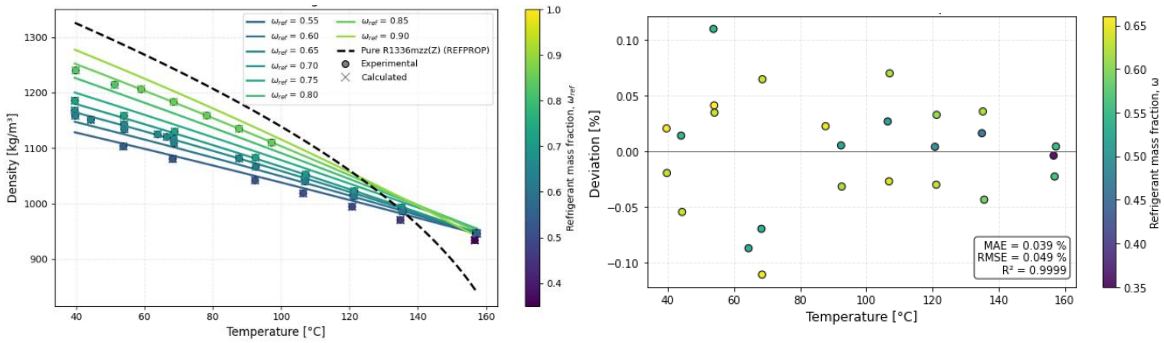

Figure 4. (a) Comparison of experimental and correlated densities using empirical model (b) Relative deviation between the empirical model predictions and experimental measurements.

4.4. Kinematic viscosity vs temperature

The kinematic viscosity was modeled using two approaches: an empirical log–log linear correlation and the ASTM D7152-type blending rule. The empirical model employs two separate coefficient sets corresponding to low ($0.55 < \omega < 0.7$) and high refrigerant mass fractions ($\omega > 0.7$), enabling it to capture the strong nonlinearity in viscosity–composition behavior with higher fidelity. As a result, this model exhibits slightly lower MAE (0.0325 cSt) and RMSE (0.0470 cSt) compared to the ASTM rule (MAE: 0.0672 cSt, RMSE: 0.0824 cSt) (Figures 5 and 6). However, this increased accuracy comes at the cost of more fitting parameters and a higher requirement for the amount and density of experimental data around the points of interest. In contrast, the ASTM blending rule provides a unified description of the entire composition range using only four coefficients, and still achieves excellent predictive capability with only marginally higher deviation. This demonstrates that the ASTM rule is both robust and sufficiently accurate for practical engineering use, whereas the empirical log–log correlation offers the best accuracy when extensive data are available.

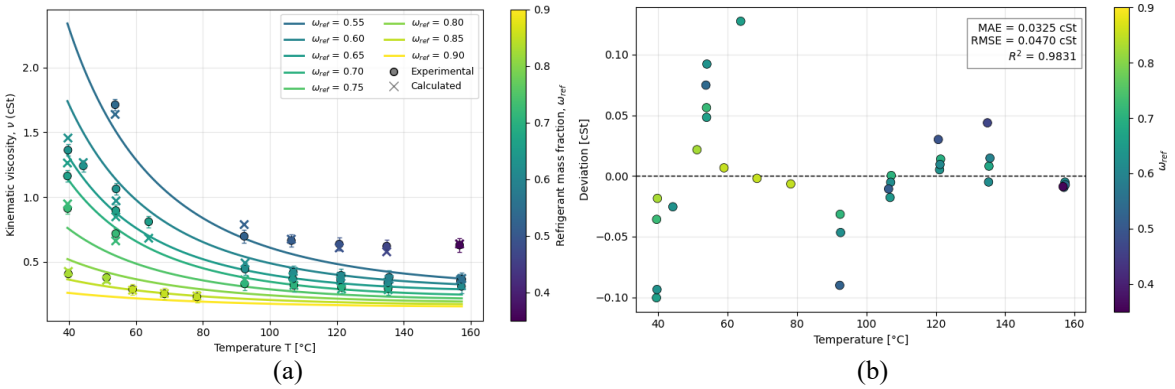

Figure 5. (a) Comparison of experimental and correlated kinematic viscosities using empirical model (b) Relative deviation between the empirical model predictions and experimental measurements

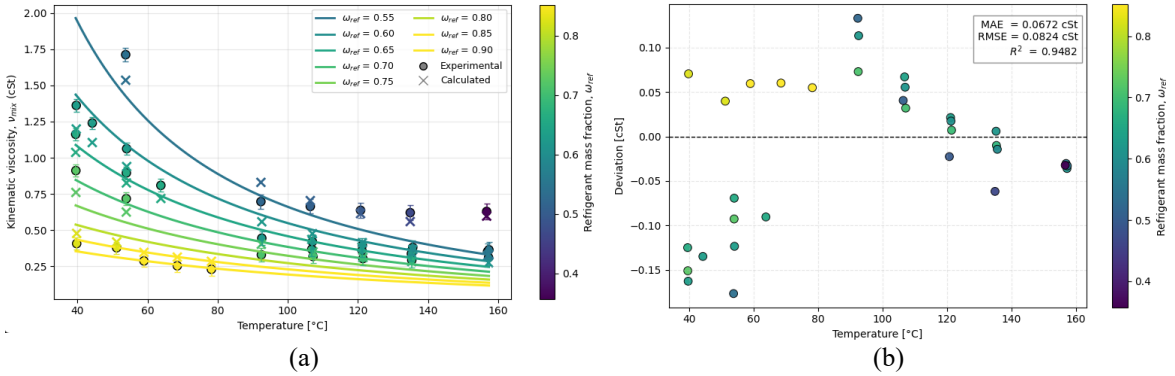

Figure 6. (a) Comparison of experimental and correlated kinematic viscosities using ASTM blending rule (b) Relative deviation between the ASTM blending rule predictions and experimental measurements

4.5. Experimental data – tabular form

Table 3 and 4 presents the measured thermophysical properties of R1336mzz(Z)–POE 380 mixtures at various refrigerant mass fractions and temperatures ranging from 40 °C to 160 °C. The experimental uncertainties were ± (0.15 + 0.002·T) ºC for temperature, ±0.2 bar for pressure, ±0.05 cP for viscosity, and ±2 kg/m³ for density.

Table 3. Density and Viscosity of R1336mzz(Z) with POE 380

Ref. mass fraction	Temperature (°C)	Viscosity (cP)	Density (kg/m^3)
0.72	39.58	1.08	1185.7
0.72	53.95	0.83	1158.3
0.71	92.46	0.36	1082.9
0.70	107.19	0.33	1052.5
0.69	121.41	0.31	1022.5
0.68	135.34	0.29	993.1
0.61	157.24	0.29	947.6
0.66	39.53	1.36	1167.7
0.66	53.98	1.02	1143.1
0.66	63.81	0.91	1124.9
0.64	106.85	0.38	1045.1
0.63	121.12	0.37	1017.2
0.62	135.23	0.33	989.3
0.56	156.95	0.33	946.8
0.63	39.69	1.58	1158.4
0.63	44.25	1.43	1151.3
0.63	54.06	1.21	1134.0
0.62	92.59	0.47	1066.4
0.62	107.01	0.44	1039.9
0.61	121.24	0.40	1013.3
0.59	135.62	0.37	986.0
0.55	157.33	0.34	945.4
0.54	53.78	1.89	1103.3
0.52	92.33	0.73	1041.7
0.51	106.41	0.68	1018.7
0.49	120.74	0.63	994.6
0.47	134.90	0.60	970.6
0.36	156.69	0.59	934.1
0.83	39.81	0.50	1240.0
0.83	51.20	0.46	1214.6
0.85	58.99	0.35	1206.1
0.85	68.49	0.30	1183.3
0.85	78.22	0.27	1158.7
0.72	39.58	1.08	1185.7
0.72	53.95	0.83	1158.3
0.71	92.46	0.36	1082.9

Table 4. Saturation pressure of R1336mzz(Z) with POE 380

Ref. mass fraction	Temperature (°C)	Saturation Pressure (bar)
0.72	39.60	1.25
0.72	54.40	2.02
0.72	69.35	3.13
0.71	93.38	5.83

0.70	108.62	8.33
0.69	123.12	11.29
0.68	137.19	14.88
0.64	150.40	19.09
0.59	160.00	22.45
0.53	68.94	3.00
0.52	93.46	5.57
0.49	122.77	10.44
0.54	44.23	1.40
0.54	54.18	1.91
0.53	62.03	2.47
0.51	108.12	7.76
0.46	137.34	13.74
0.32	159.69	19.64
0.63	44.43	1.50
0.62	93.68	5.85
0.61	108.44	8.18
0.61	123.01	11.09
0.59	137.61	14.79
0.63	54.41	2.05
0.54	159.82	21.95
0.85	39.61	1.21
0.85	49.48	1.70
0.85	59.26	2.30
0.85	69.25	3.07
0.85	79.04	4.04
0.85	88.84	5.22
0.85	98.67	6.68
0.72	39.60	1.25
0.72	54.40	2.02
0.72	69.35	3.13
0.71	93.38	5.83

5. Conclusion

This study presented a comprehensive experimental investigation of the thermophysical properties of R1336mzz(Z)–POE 380 mixtures across a wide temperature range (40–160 °C) and refrigerant mass fractions (0.55–0.9), using a high-temperature measurement setup capable of operation up to 190 °C. The measured data for saturation pressure, density, and viscosity were successfully represented using empirical correlations based on the widely used empirical equations, achieving excellent agreement with experimental values for the refrigerant mass fraction range of 0.55–0.9. The viscosity–temperature behavior was further evaluated using the ASTM D7152 blending rule, and the two models were compared to assess predictive capability. The results highlight the strong influence of refrigerant concentration on mixture properties, especially at elevated temperatures, and the developed correlations provide reliable inputs for component modeling and high-temperature heat pump cycle simulations employing low-GWP refrigerant–lubricant mixtures.

Acknowledgements

We would like to express our gratitude to Shrieve lubricants and ASHRAE for their support in this project.

References

[1] Jouhara, H., Żabnieńska-Góra, A., Delpech, B., Olabi, V., El Samad, T., Sayma, A., 2022. *High-temperature heat pumps: Fundamentals, modelling approaches and applications. Energy* 239, 122219.

[2] Jiang, J., Hu, B., Wang, R.Z., Deng, N., Cao, F., Wang, C.C., 2022. *A review and perspective on industry high-temperature heat pumps. Renewable and Sustainable Energy Reviews* 161, 112106.

[3] Mateu-Royo, C., Arpagaus, C., Mota-Babiloni, A., Navarro-Esbrí, J., Bertsch, S.S., 2021. *Advanced high temperature heat pump configurations using low GWP refrigerants for industrial waste heat recovery: A comprehensive study. Energy Conversion and Management* 229, 113752.

[4] Brückner, S., Liu, S., Miró, L., Radspieler, M., Cabeza, L.F., Lävenmann, E., 2015. *Industrial waste heat recovery technologies: An economic analysis of heat transformation technologies. Applied Energy* 151, 157–167.

[5] Frate, G.F., Ferrari, L., Desideri, U., 2019. *Analysis of suitability ranges of high temperature heat pump working fluids. Applied Thermal Engineering* 150, 628–640.

[6] Mota-Babiloni, A., Mateu-Royo, C., Navarro-Esbrí, J., Molés, F., Amat-Albuixech, M., Barragán-Cervera, Á., 2018. *Optimisation of high-temperature heat pump cascades with internal heat exchangers using refrigerants*

[7] Dawo, F., Fleischmann, J., Kaufmann, F., Schifflechner, C., Eyerer, S., Wieland, C., Spliethoff, H., 2021. *R1224yd(Z), R1233zd(E) and R1336mzz(Z) as replacements for R245fa: Experimental performance, interaction with lubricants and environmental impact. Applied Energy* 288, 116661.

[8] Conde, M.R., 1996. *Estimation of thermophysical properties of lubricating oils and their solutions with refrigerants: An appraisal of existing methods. Applied Thermal Engineering* 16 (1), 53–61.

[9] Marsh, K.N., Kandil, M.E., 2002. *Review of thermodynamic properties of refrigerants + lubricant oils. Fluid Phase Equilibria* 199 (1–2), 319–334

[10] Karnaz, J., Seeton, C., 2018. *Evaluation of lubricant properties and refrigerant interaction.* In: *Proceedings of the International Compressor Engineering Conference*, Purdue University, West Lafayette, IN, USA. Paper 1681.

[11] Henderson, D.R. (1994). Solubility, viscosity and density of refrigerant/lubricant mixtures.

[12] ASTM Standard D7152. (2005e1). Standard Practice for Calculating Viscosity of a Blend of Petroleum Product*s*. ASTM International, West Conshohocken, PA.

[13] ASHRAE, 2022. ASHRAE Standard 15-2022: Safety Standard for Refrigeration Systems. American Society of Heating, Refrigerating and Air-Conditioning Engineers, Atlanta, GA.

[14] ASHRAE, 2022. ASHRAE Standard 34-2022: Designation and Safety Classification of Refrigerants. American Society of Heating, Refrigerating and Air-Conditioning Engineers, Atlanta, GA

[15] Lemmon, E. W., Bell, I. H., Huber, M. L., & McLinden, M. O. (2018). *NIST Standard Reference Database 23: Reference Fluid Thermodynamic and Transport Properties (REFPROP), Version 10.0*. National Institute of Standards and Technology, Gaithersburg, MD

[16] Venkatesan, G. B., & Barta, R. B. (2025). *Experimental investigation of thermophysical properties of low-global warming potential refrigerant–lubricant mixtures across extreme temperature ranges*. 7th IIR Conference on Thermophysical Properties and Transfer Processes of Refrigerants, College Park, MD, USA.

[17] Seeton, C.J., 2009. CO_2-lubricant two-phase flow patterns in small horizontal wetted wall channels ; the effects of refrigerant/lubricant thermophysical properties. PhD Dissertation, University of Illinois at Urbana-Champaign, Urbana, Illinois.